Ultrathin fluid films confined to a chemically heterogeneous slit-shaped nanopore

Martin Schoen*
Institut für Theoretische Physik, Sekretariat PN 7-1, Fachbereich Physik, Technische Universität Berlin, Hardenbergstraße 36, D-10623 Berlin, Germany

Dennis J. Diestler†
Department of Agronomy, University of Nebraska–Lincoln, Lincoln, Nebraska 68583-0915
(Received 13 May 1997)

The properties of a molecularly thin film of Lennard-Jones (LJ) (12,6) fluid confined to a chemically heterogeneous slit-shaped pore were investigated by the grand canonical ensemble Monte Carlo (GCEMC) method. The slit-shaped pore comprises two identical plane-parallel solid substrates, each of which consists of alternating strips of LJ(12,6) solid of two types: strongly adsorbing and weakly adsorbing. With substrates aligned so that strips of the same type oppose each other, GCEMC was used to compute equilibrium properties of the film as functions of the distance s_z between the substrates. Results are compared for two well depths ϵ_{fs} of the LJ(12,6) potential between molecules in the film and those in the strongly adsorbing strip. Variations in tensions, mean film density, and isothermal compressibility as functions of s_z are correlated with structural changes in the film and with its phase behavior. In both cases, when the substrates are sufficiently close together, liquid bridges exist between the opposing strong strips, surrounded by dilute gas over the weak ones. The stronger substrate (i.e., the one with the greater value of ϵ_{fs}) is capable of stabilizing a liquidlike phase that fills the whole pore over a certain range of s_z, then abruptly evaporates beyond a critical value of s_z, to leave nanodroplets clinging to the strong strips. For the weaker substrate, however, the liquid bridges collapse to form nanodroplets directly, without the intermediate appearance of a liquid pore-filling phase.
[S1063-651X(97)07910-5]

PACS number(s): 61.20.Ja, 61.20.Ne, 68.45.−v, 64.70.Fx

I. INTRODUCTION

The deportment of fluids confined to spaces of molecular or nanoscopic dimensions has profound consequences for natural phenomena such as the swelling of clay minerals [1,2] and the functioning of living cells [3], as well as for technological processes such as lubrication [4] and the manufacture and operation of microscopic machines [5]. We focus in this article on the properties of ultrathin fluid films confined to a single, definitively characterized slit-shaped pore (i.e., a thin film of fluid sandwiched between two plane-parallel solid substrates). Such films can be studied in the laboratory more or less directly by means of the surface forces apparatus (SFA) [6–8], the heart of which comprises two parallel mica sheets that can be manipulated with nearly molecular precision. Analogous virtual investigations can be performed by computer simulation [9–11]. Indeed, the primary purpose of this paper is to present detailed results of such simulations of a slit-shaped pore whose walls are chemically patterned on the nanoscale.

With two exceptions [12,13] prior investigations have dealt with walls that are smooth on the nanoscale. The film, a pure substance, is assumed to be in thermodynamic equilibrium with the bulk fluid at fixed temperature T and pressure. The mechanical state of the film, which is inhomogeneous and anisotropic, is specified by a set of strains (in the simplest case, the distance between the walls, s_z, and their lateral alignment or registry) or their conjugate stresses (the normal stress T_{zz} is conjugate to s_z and the shear stress is conjugate to registry). Here and below we take the film-substrate interface to be perpendicular to the z axis. The applied load is observed (in both SFA measurements [14,15] and simulations [9–11,16]) to oscillate between attraction and repulsion with a period of about one diameter of the film molecule (σ) as s_z increases from 2σ to about 10σ at constant T and chemical potential μ. Monte Carlo simulations in the grand canonical ensemble (GCEMC, fixed T, μ, and s_z) [9,10,17–19] and in the grand isostress ensemble [16,20,21] demonstrate that the fluid piles up in layers parallel with the walls and that, in coincidence with the oscillations in T_{zz}, whole layers of fluid abruptly enter the pore. This stratification, due to constraints on the packing of molecules against the rigid planar walls, thus accounts for the oscillatory dependence of T_{zz} on s_z [22]. Grand canonical Monte Carlo simulations [23,24] of a monatomic film between walls comprising like atoms fixed in the configuration of the face centered cubic (fcc) (100) plane show that if the walls are in the right registry they can induce freezing of a molecularly thin film. The frozen film resists shearing (i.e., the walls stick) until a critical shear strain is surpassed, whereupon the film melts and the walls slip. This effect has been invoked to explain stick-slip lateral movement observed by the SFA [25,26].

Although SFA experiments referred to above, and the analogous computer simulations, involve substrates that are structurally and chemically *homogeneous* (in lateral dimensions) on the nanoscale, relatively recent advances in miniaturization have made feasible the construction of substrates

*Electronic address: m.schoen@physik.tu-berlin.de
†Electronic address: agro016@unlvm.unl.edu

possessing prescribed heterogeneities [27,28]. It is therefore of some urgency to investigate the influence of nanoscale heterogeneities on the behavior of a fluid film in a slit-shaped pore. Indeed, in an earlier GCEMC simulation [12] we examined the effects of nanoscale *structural* heterogeneity. We took one wall to be a fcc (100) plane and the other a fcc (100) plane scored with regularly spaced rectilinear grooves several σ wide. Film and wall molecules were assumed identical. When s_z is fixed at about 2σ and the walls are in proper registry, the film comprises solid and fluid portions in thermodynamic equilibrium, that is, fluid-filled nanocapillaries (the grooves) alternating with solid columns. Epitaxial freezing of the film is promoted by the molecular-scale templates of the strips between the grooves, just as it is in the case of walls *structurally* smooth on the nanoscale [19–24]. In the grooves, however, the template is so weak that the film remains fluid there. Thus it is clear that a purely structural heterogeneity on the nanoscale can induce phase coexistence in confined films.

We present here results of a GCEMC study designed to determine whether strictly *chemical* heterogeneity on the nanoscale might engender phase coexistence. Koch *et al.* [29] briefly reviewed previous work on the nature of fluid layers adsorbed on single chemically patterned substrates. To divorce chemical from structural effects, we adopted a simple chemically striped smooth-wall model (i.e., each wall consists of strongly adsorbing strips alternating with weakly adsorbing ones). Our notion is that film molecules should tend to concentrate over the strong strips, leaving the film over the weak ones at lower density. In other words, we would expect the strong strips to become wet and the weak ones to remain dry. This would result in a nanoscopic liquid-vapor equilibrium, that is, liquid over the strong strips separated from gas over the weak ones by interfaces parallel to the strips and perpendicular to the walls. A situation akin to the one just described has indeed been observed recently by Röcken and Tarazona [30], who studied capillary condensation in slit-shaped pores with chemically corrugated walls using a simple lattice-gas model. In their model the wall is represented by a potential field that oscillates sinusoidally between attraction and repulsion in one transverse direction (x) and extends about 1σ from the plane of the wall.

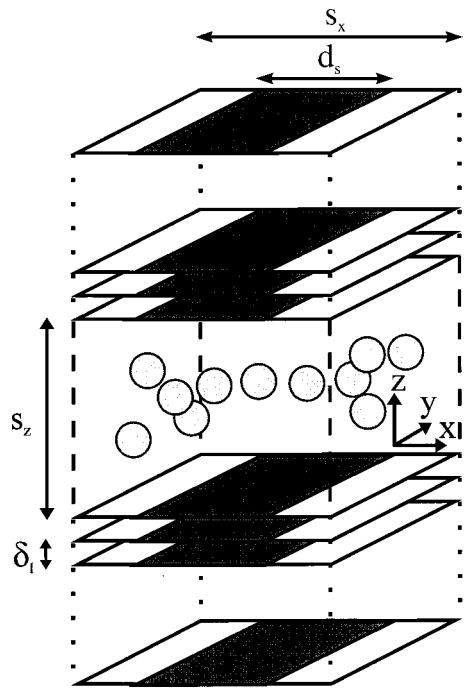

FIG. 1. Scheme of a simple fluid confined by a chemically heterogeneous model pore. Film molecules (gray spheres) are spherically symmetric. Each substrate consists of a sequence of crystallographic planes separated by a distance δ_f along the z axis. The surface planes of the two opposite substrates are separated by a distance s_z. Periodic boundary conditions are imposed in the x and y directions (see text).

II. THE MODEL

A. Mean-field description of the substrate potential

Our model system, sketched in Fig. 1, consists of a film composed of spherically symmetric molecules which is sandwiched between the surfaces of two solid substrates. The substrate surfaces are planar, parallel, and separated by a distance s_z along the z axis of the coordinate system. The substrates are semi-infinite in the z direction, occupying the half spaces $s_z/2 \leqslant z \leqslant \infty$ and $-\infty \leqslant z \leqslant -s_z/2$, and infinite in the x and y directions. Each substrate comprises alternating slabs of two types: strongly adsorbing and weakly adsorbing. The ''strong'' and ''weak'' slabs have widths d_s and d_w, respectively, in the x direction and are infinite in the y direction. The system is thus periodic in the x direction of period d_s+d_w and is translationally invariant in the y direction. In practice we take the system to be a finite piece of the film, imposing periodic boundary conditions [31] on the planes $x = \pm s_x/2$ and $y = \pm s_y/2$.

The substrates are in registry in that slabs of the same type are exactly opposite each other. Substrate atoms are assumed to be of the same ''diameter'' (σ) and to occupy the sites of the fcc lattice [the substrate surfaces are taken to be (100) planes] having lattice constant ℓ, which is taken to be the same for both species. Thus substrate species are distinguished only by the strength of their interaction with film molecules. We assume the total potential energy to be a sum of pairwise additive LJ(12,6) potentials, all of which have the form

$$u(r) = 4\epsilon\left[\left(\frac{\sigma}{r}\right)^{12} - \left(\frac{\sigma}{r}\right)^{6}\right], \tag{1}$$

where ϵ is the well depth, σ the molecular ''diameter,'' and r the distance between the centers of a pair of particles (i.e., film molecules or substrate atoms). For the interaction between a pair of film molecules $\epsilon = \epsilon_{ff}$ [i.e., $u_{ff}(r)$]. The nanoscale heterogeneity of the substrate is characterized by $\epsilon = \epsilon_{fs}$ [i.e., $u_{fs}(r)$] for the interaction of a film molecule with a substrate atom in the strong (central) slab, and by $\epsilon = \epsilon_{fw}$ [i.e., $u_{fw}(r)$] for the interaction of a film molecule with a substrate atom in either of the two weak (outer) slabs (see Fig. 1). We take $\epsilon_{fs} \geqslant \epsilon_{ff}$ and $\epsilon_{fw} \leqslant \epsilon_{ff}$ (see Sec. IV for specific values).

Since we are concerned in this article with the effects of chemical heterogeneity at the nanoscale on the behavior of

the confined film, we expect the details of the atomic structure not to matter greatly for our purpose. Therefore we adopt a mean-field representation of the interaction of a film molecule with the substrate, which we obtain by averaging the film-substrate interaction potential over positions of substrate atoms in the x-y plane. The resulting mean-field potential can be expressed as

$$\begin{aligned}\Phi^{[k]}(x,z;d_s,s_x,s_z)&=n_A\sum_{m=-\infty}^{\infty}\sum_{m'=0}^{\infty}\int_{-\infty}^{\infty}dy'\left\{\int_{-s_x/2+ms_x}^{-d_s/2+ms_x}dx'\,u_{fw}(|\mathbf{r}-\mathbf{r}'|)\right.\\&+\int_{-d_s/2+ms_x}^{d_s/2+ms_x}dx'\,u_{fs}(|\mathbf{r}-\mathbf{r}'|)\\&\left.+\int_{d_s/2+ms_x}^{s_x/2+ms_x}dx'\,u_{fw}(|\mathbf{r}-\mathbf{r}'|)\right\}.\end{aligned}\tag{2}$$

In Eq. (2) $n_A=2/\ell^2$ is the areal density of the (100) plane of the fcc lattice. The position of a film molecule is denoted by $\mathbf{r}$ and $\mathbf{r}'=(x',y',z'=\pm s_z/2\pm m'\delta_\ell)$ represents the position of a substrate atom, where $-$ refers to the lower ($k=1$), $+$ to the upper ($k=2$) substrate, and δ_ℓ is the spacing between successive crystallographic planes in $\pm z$ direction. We note that since all features of the substrate at the atomic scale have been washed out in $\Phi^{[k]}$, our mean-field model cannot account properly for solid formation, which, according to the discussion in Sec. I, is strongly influenced by the atomic structure of the substrate.

By interchanging the order of integration and introducing the transformation

$$\begin{aligned}x'&\to x''=x-x',\\y'&\to y''=y-y',\\z'&\to z''=z-(\pm s_z/2\pm m'\delta_\ell)\end{aligned}\tag{3}$$

we can rewrite the integrals on the right-hand side of Eq. (2) as

$$\begin{aligned}&\int_a^b dx'\int_{-\infty}^{\infty}dy'\,u(|\mathbf{r}-\mathbf{r}'|)\\&\quad=-4\epsilon\int_{x-a}^{x-b}dx''\int_{-\infty}^{\infty}dy''\left[\left(\frac{\sigma^2}{x''^2+y''^2+z''^2}\right)^6\right.\\&\qquad\left.-\left(\frac{\sigma^2}{x''^2+y''^2+z''^2}\right)^3\right],\end{aligned}\tag{4}$$

where a and b refer to integration limits and u and ϵ correspond to u_{fs} and ϵ_{fs} or to u_{fw} and ϵ_{fw}, depending on a and b. The definite integral over y'' can be found in standard tabulations (see, for example, no. 60 in [32]). Thus Eq. (4) simplifies to

$$\begin{aligned}&4\epsilon\int_{x-a}^{x-b}dx''\int_{-\infty}^{\infty}dy''\left[\left(\frac{\sigma^2}{x''^2+y''^2+z''^2}\right)^6\right.\\&\qquad\left.-\left(\frac{\sigma^2}{x''^2+y''^2+z''^2}\right)^3\right]\\&\quad=\frac{3\pi\epsilon\sigma}{2}\int_{x-a}^{x-b}dx''[I_1(x'',z'';d_s,s_x,s_z)\\&\qquad-I_2(x'',z'';d_s,s_x,s_z)],\end{aligned}\tag{5}$$

where

$$I_1(x'',z''):=\frac{21}{32}\sqrt{\left(\frac{\sigma^2}{R}\right)^{11}}\tag{6}$$

and

$$I_2(x'',z''):=\sqrt{\left(\frac{\sigma^2}{R}\right)^{5}},\tag{7}$$

with

$$R:=x''^2+z''^2.\tag{8}$$

The remaining integration over x'' can also be carried out analytically (see, for example, no. 244 in [32]). A tiresome computation yields

$$\begin{aligned}\int_{x-a}^{x-b}dx''I_1(x'',z'')&=\frac{21}{32}\int_{x-a}^{x-b}dx''\sqrt{\left(\frac{\sigma^2}{R}\right)^{11}}\\&=:\frac{21\sigma}{32}I_3(x'',z'';d_s,s_x,s_z)\Big|_{x''=x-a}^{x''=x-b}\\&=\frac{21\sigma}{32}\frac{x''\sigma^{10}}{9z''^2\sqrt{R^9}}\left[1+\frac{8}{7}S+\frac{48}{35}S^2+\frac{64}{35}S^3\right.\\&\qquad\left.+\frac{128}{35}S^4\right]\Big|_{x''=x-a}^{x''=x-b}\end{aligned}\tag{9}$$

and

$$\begin{aligned}\int_{x-a}^{x-b}dx''I_2(x'',z'')&=\int_{x-a}^{x-b}dx''\sqrt{\left(\frac{\sigma^2}{R}\right)^{5}}\\&=:\sigma I_4(x'',z'';d_s,s_x,s_z)|_{x''=x-a}^{x''=x-b}\\&=\sigma\frac{x''\sigma^4}{3z''^2\sqrt{R^3}}[1+2S]\Big|_{x''=x-a}^{x''=x-b},\end{aligned}\tag{10}$$

where the dimensionless quantity S is given by

$$S:=\frac{R}{z''^2}.\tag{11}$$

To simplify the expressions, we define the auxiliary function

$$\Delta(x'',z'';d_s,s_x,s_z):=\frac{21}{32}I_3(x'',z'';d_s,s_x,s_z)$$
$$-I_4(x'',z'';d_s,s_x,s_z). \qquad (12)$$

Combining the expressions in Eqs. (2), (5), (9), (10), and (12), we have finally for the potential energy of a film molecule in the mean field of the substrate k $(=1,2)$

$$\Phi^{[k]}=-\frac{3\pi}{2}n_A\sigma^2\sum_{m=-\infty}^{\infty}\sum_{m'=0}^{\infty}\left\{(\epsilon_{fw}-\epsilon_{fs})\right.$$
$$\times\Delta\left(x+\frac{d_s}{2}-ms_x,\ \frac{s_z}{2}+m'\delta_{/\!/}\pm z\right)$$
$$-(\epsilon_{fw}-\epsilon_{fs})\Delta\left(x-\frac{d_s}{2}-ms_x,\ \frac{s_z}{2}+m'\delta_{/\!/}\pm z\right)$$
$$-\epsilon_{fw}\left[\Delta\left(x+\frac{s_x}{2}-ms_x,\ \frac{s_z}{2}+m'\delta_{/\!/}\pm z\right)\right.$$
$$\left.\left.-\Delta\left(x-\frac{s_x}{2}-ms_x,\ \frac{s_z}{2}+m'\delta_{/\!/}\pm z\right)\right]\right\}, \qquad (13)$$

where the sign on z is chosen according to the convention $+\leftrightarrow k=1$ and $-\leftrightarrow k=2$ (see Fig. 1).

Before discussing the implementation of Eq. (13) in the GCEMC simulation, we comment briefly on the properties of the *whole* film-substrate potential $\Phi=\Phi^{[1]}+\Phi^{[2]}$ that follow strictly from considerations of symmetry. When the z coordinate of the film molecule is reflected through the mirror plane $z=0$, $-z$ in the arguments $z''=s_z/2+m'\delta_{/\!/}\pm z$ of $\Phi^{[1]}$ changes to $+z$ in the arguments of $\Phi^{[2]}$ and vice versa. That is, $\Phi^{[1]}(x,-z)\rightarrow\Phi^{[2]}(x,z)$ and vice versa. The sum Φ is therefore invariant under reflection in the $z=0$ plane. Likewise, Φ is invariant under reflection in the x plane, although the proof involves more subtle interconversions. For example, under the transformation $x\rightarrow -x$ the first term in braces (for m) is converted into the second term in braces (for $-m$). Likewise, the third term [in square brackets in Eq. (13)] is converted into the fourth term. Of course, since the potential is periodic in x, of period s_x, we need represent the whole mean-field film-substrate potential in only one quadrant (say, $0\leqslant x\leqslant s_x/2$, $0\leqslant z\leqslant s_z/2$) of the $x-z$ plane.

B. Computation of film-wall contribution to configurational energy

The generation of a GCEMC Markov chain of configurations $\mathbf{r}^{N_f}:=\{\mathbf{r}_1,\mathbf{r}_2,\ldots,\mathbf{r}_{N_f}\}$ is governed by the (change in) configurational energy [33], where N_f is the number of film molecules. For the present system the configurational energy U can be written as

$$U=\frac{1}{2}\sum_{i=1}^{N_f}\sum_{j\neq i=1}^{N_f}u_{ff}(r_{ij})+\sum_{k=1}^{2}\sum_{i=1}^{N_f}\Phi^{[k]}(x_i,z_i;d_s,s_x,s_z)$$
$$=:U_{FF}+U_{FS}, \qquad (14)$$

where u_{ff} is given in Eq. (1), $\Phi^{[k]}$ in Eq. (13), and $r_{ij}:=|\mathbf{r}_i-\mathbf{r}_j|$ is the distance between the centers of film molecules i and j located at $\mathbf{r}_i$ and $\mathbf{r}_j$, respectively. Equation (14) also defines the film-film and film-substrate contributions U_{FF} and U_{FS} to U. To implement the expression for $\Phi^{[k]}$ in Eq. (13), we truncate the infinite summations according to $\Sigma_{m=-\infty}^{\infty}\Sigma_{m'=0}^{\infty}\rightarrow\Sigma_{m=-M}^{M}\Sigma_{m'=0}^{M'}$, where integers M and M' are large enough to yield $\Phi^{[k]}$ with a prescribed precision. For a system size of $s_x^*:=s_x\sigma^{-1}\geqslant 10$ and a lattice spacing of $\delta_{/\!/}^*:=\delta_{/\!/}\sigma^{-1}=1.0$, we find that $M=2$ and $M'=50$ are large enough to give $\Phi^{[k]}$ to a precision of 0.3% regardless of the position of a film molecule with respect to the substrate.

However, M and M' are still too large to employ the truncated version of Eq. (13) directly in each GCEMC step. Tests show that for $M=2$ and $M'=50$ the evaluation of $\Phi^{[k]}$ for a *single* film molecule requires approximately the same amount of computer time as the computation of U_{FF} for $N_f=100$, so that a GCEMC simulation of a typical length of 10^6 or 10^7 configurations would be prohibitively expensive. Instead of computing $\Phi^{[k]}$ during each step of the GCEMC simulation we adopted the following procedure. Prior to the simulation we computed $\Phi^{[k]}$ by the truncated version of Eq. (13) and stored it at the nodes of a square grid $\{x_k,z_k\}_{k=1,\ldots,K}$ in the quadrant $0\leqslant x\leqslant s_x/2$, $0\leqslant z\leqslant s_z/2$. During the simulation the value of $\Phi^{[k]}$ at the the actual (instantaneous) position (x_i,z_i) of film molecule i (which does not necessarily coincide with any node) is obtained by bilinear interpolation [34] among the values of $\Phi^{[k]}$ at the four nearest-neighbor nodes of (x_i,z_i).

We tested the interpolation scheme for a special case in which $\Phi^{[k]}$ can be readily evaluated during each GCEMC step. The substrate consists of a single, chemically homogeneous plane for which we set $\epsilon_{fs}=\epsilon_{fw}=\epsilon_{ff}$. Thus the discrete sum on m and piecewise integrations over the strips are replaced by a single integration on x' from $-\infty$ to ∞. The summation on m' also reduces to a single term $m'=0$. Under these conditions Eq. (2) can be rewritten as

$$\Phi^{[k]}(z;s_z)=4\epsilon_{ff}n_A\int_0^{2\pi}d\phi\int_0^{\infty}d\rho\,\rho\left[\left(\frac{\sigma^2}{\rho^2+z''^2}\right)^6\right.$$
$$\left.-\left(\frac{\sigma^2}{\rho^2+z''^2}\right)^3\right] \qquad (15)$$

in cylindrical coordinates, so that the integrations on ϕ and ρ can be carried out in closed form to yield

$$\Phi^{[k]}(z;s_z)=2\pi\epsilon_{ff}n_A\sigma^2\left[\frac{2}{5}\left(\frac{\sigma}{z\pm s_z/2}\right)^{10}-\left(\frac{\sigma}{z\pm s_z/2}\right)^4\right], \qquad (16)$$

where $(+\leftrightarrow k=1,\ -\leftrightarrow k=2)$. Employing a mesh of $\delta_x^*=\delta_z^*=0.025$, corresponding to $K=7.6\times10^3$ $(s_x^*=10,\ s_z^*=1.9)$ for the smallest substrate separation and $K=5.0\times10^4$ $(s_x^*=10,\ s_z^*=12.50)$ for the largest, we compare (see Table I) results obtained using the interpolation scheme [Eq. (13)] with those based on direct evaluation of the potential given by Eq. (16). It is noteworthy that the agreement is good, even for film-film (FF) and film-substrate (FS) contributions to the normal component of the stress tensor T_{zz}

TABLE I. Comparison of interpolation [truncated version of Eq. (13)] and direct evaluation [Eq. (16)] of film-substrate potential energy for various properties of a film confined by substrates consisting of single, chemically homogeneous planes. Entries, given in dimensionless units defined at the beginning of Sec. IV, refer to simulations based on either direct evaluation (D) or interpolation (I).

s_z^*	$-\mu^*$	$\langle N\rangle$		$-\langle U_{FF}^*/N\rangle$		$-\langle U_{FS}^*/N\rangle$		$-T_{zz,FF}^*$		$-T_{zz,FS}^*$	
		D	I	D	I	D	I	D	I	D	I
3.00	9.56	98.6	98.5	3.676	3.668	2.920	2.912	1.09	1.10	0.21	0.20
2.70	9.46	79.7	79.8	3.086	3.088	3.021	3.013	2.45	2.44	3.16	3.20
2.20	9.26	50.3	50.3	2.103	2.113	4.860	4.858	0.42	0.42	−1.53	−1.54

(defined in Sec. III A), which are particularly sensitive to numerical inaccuracies in case the magnitude of these contributions is small.

III. STATISTICAL THERMODYNAMICS OF MOLECULARLY THIN FILMS BETWEEN CHEMICALLY STRIPED WALLS

To compute thermomechanical properties of confined films, we employ the grand canonical ensemble, in which a thermodynamic equilibrium state of the film is uniquely specified by temperature T, chemical potential μ, and volume $V=As_z$. Thus the film is materially and thermally open to its environment, as is the film in a corresponding SFA experiment. From a formal thermodynamic perspective we regard the *system* as a finite lamella of the (infinite) film having dimensions $s_x\times s_y\times s_z$ [35,36]. The environment therefore comprises the remainder of the film plus the substrates. The lamella is bounded in the normal (z) direction by the substrate surfaces and in the transverse directions by two pairs of planes ($x=\pm s_x/2$, $y=\pm s_y/2$). Through movements of the substrate and these planes, which function as imaginary pistons, the lamella can do work on its environment and vice versa [36]. An infinitesimal, reversible transformation of the lamella is governed by Gibbs's fundamental relation in differential form [35,36]

$$\begin{aligned} d\Omega &= -SdT - N_l d\mu + T_{xx}s_y s_z ds_x + T_{yy}s_x s_z ds_y + T_{zz}s_x s_y ds_z \\ &= -SdT - N_l d\mu + dW, \end{aligned} \tag{17}$$

where $\Omega := U - TS - \mu N_l$ is the grand potential, S is the entropy, U is the internal energy, N_l is the number of molecules accommodated by the lamella, and $T_{\alpha\alpha}$ ($\alpha=x,y,z$) are diagonal elements of the stress tensor $\mathbf{T}$ associated with the exchange of compressional work

$$dW = \sum_\alpha A_\alpha T_{\alpha\alpha} ds_\alpha \tag{18}$$

between the lamella and its environment. In Eq. (18) A_α is the area of the α directed face of the lamella. The absence of off-diagonal elements of $\mathbf{T}$ signifies that we ignore work due to shear. Under the conditions of fixed T, μ, s_x, and s_z, Ω is a homogeneous function of degree one of s_y, so that Euler's theorem applied to Eq. (17) yields

$$\Omega = T_{yy} V_l, \tag{19}$$

where $V_l = s_x s_y s_z$ is the volume of the lamella.

The linkage to the molecular scale is the well-known statistical thermodynamic relation [37]

$$\Omega(T,\mu,V_l) = -\beta^{-1} \ln \Xi(T,\mu,V_l), \tag{20}$$

where $\beta := 1/k_B T$ (k_B Boltzmann's constant), and

$$\Xi(T,\mu,V_l) = \sum_{N_l=0}^{\infty} \frac{\exp[\beta\mu N_l]}{N_l!\,\Lambda^{3N_l}} Z_{N_l}(T,V_l) \tag{21}$$

is the grand canonical partition function for a classical system in which the molecules possess only translational degrees of freedom. In Eq. (21) Λ denotes the thermal de Broglie wavelength [38] and

$$\begin{aligned} Z_{N_l}(T,V_l) &= \int_{V_l^{N_l}} d\mathbf{r}^{N_l} \exp[-\beta U] \\ &= \prod_{i=1}^{N_l} \int_{-s_x/2}^{s_x/2} dx_i \int_{-s_y/2}^{s_y/2} dy_i \int_{-s_z/2}^{s_z/2} dz_i \\ &\quad \times \exp[-\beta(U_{FF}+U_{FS})] \end{aligned} \tag{22}$$

is the configurational integral.

A. Stress tensor

From Eq. (17) we have the purely thermodynamic expression

$$A_\alpha T_{\alpha\alpha} = \left(\frac{\partial\Omega}{\partial s_\alpha}\right)_{T,\mu,s_\beta}. \tag{23}$$

Combining Eq. (23) with the statistical expressions given in Eqs. (20) and (22), we obtain

$$T_{\alpha\alpha} = -(A_\alpha \beta \Xi)^{-1} \sum_{N_l=0}^{\infty} \frac{\exp[\beta\mu N_l]}{N_l!\,\Lambda^{3N_l}} \left(\frac{\partial Z_{N_l}}{\partial s_\alpha}\right)_{T,s_\beta}. \tag{24}$$

To evaluate the partial derivative of the configurational integral, we follow the procedure of Hill [39] and transform the variables of integration in Eq. (22) according to

$$\begin{aligned} x &\to \tilde{x} = x s_x^{-1}, \\ y &\to \tilde{y} = y s_y^{-1}, \\ z &\to \tilde{z} = z s_z^{-1}. \end{aligned} \tag{25}$$

Equation (24) can then be rewritten as

$$T_{\alpha\alpha}=-(A_\alpha\beta\Xi)^{-1}\sum_{N_l=0}^{\infty}\frac{\exp[\beta\mu N_l]}{N_l!\Lambda^{3N_l}}\times\frac{\partial}{\partial s_\alpha}\Bigg[(s_x s_y s_z)^{N_l}\prod_{i=1}^{N_l}\int_{-1/2}^{1/2}d\tilde{x}_i\int_{-1/2}^{1/2}d\tilde{y}_i\int_{-1/2}^{1/2}d\tilde{z}_i\times\exp[-\beta(U_{FF}+U_{FS})]\Bigg]. \tag{26}$$

Scaling via Eq. (25) affects U_{FF} through Eqs. (1), (14), and

$$r_{ij}=[s_x^2(\tilde{x}_i-\tilde{x}_j)+s_y^2(\tilde{y}_i-\tilde{y}_j)+s_z^2(\tilde{z}_i-\tilde{z}_j)]^{1/2} \tag{27}$$

and U_{FS} through Eqs. (13) and (14). According to the product rule, the differentiation in Eq. (26) yields three terms, which we group as

$$T_{\alpha\alpha}=T_{\alpha\alpha,FF}+T_{\alpha\alpha,FS}, \tag{28}$$

thus defining the film-film contribution by

$$\begin{aligned}T_{\alpha\alpha,FF}&=-\frac{\langle N_l\rangle}{\beta V_l}+\frac{1}{2V_l\Xi}\sum_{N_l=0}^{\infty}\frac{\exp[\beta\mu N_l]}{N_l!\Lambda^{3N_l}}\times\int_{V_l^{N_l}}d\mathbf{r}^{N_l}\exp[-\beta U]\sum_{i=1}^{N_l}\sum_{j\neq i}^{N_l}u'(r_{ij})\frac{\alpha_{ij}^2}{r_{ij}}\\&=-\frac{\langle N_l\rangle}{\beta V_l}+\frac{1}{V_l\Xi}\sum_{N_l=0}^{\infty}\frac{\exp[\beta\mu N_l]}{N_l!\Lambda^{3N_l}}\times\int_{V_l^{N_l}}d\mathbf{r}^{N_l}\exp[-\beta U]W_{\alpha\alpha}\\&=-\frac{\langle N_l\rangle}{\beta V_l}+\frac{1}{V_l}\sum_{N_l=0}^{\infty}\int_{V_l^{N_l}}d\mathbf{r}^{N_l}f_{T,\mu,V_l}(\mathbf{r}^{N_l};N_l)W_{\alpha\alpha}\\&=-\frac{\langle N_l\rangle}{\beta V_l}+\frac{\langle W_{\alpha\alpha}\rangle}{V_l}.\end{aligned} \tag{29}$$

In Eq. (29) $W_{\alpha\alpha}$ is Clausius' virial [39], $\alpha_{ij}:=\alpha_i-\alpha_j$ ($\alpha=x$, y or z), and $u'_{ff}(r):=du_{ff}/dr$. The last line of Eq. (29) implicitly defines the probability density function $f_{T,\mu,V_l}(\mathbf{r}^{N_l};N_l)$ of the grand canonical ensemble. Similarly, one finds for the film-substrate contribution in Eq. (28)

$$\begin{aligned}T_{xx,FS}&=-\frac{1}{V_l}\sum_{N_l=0}^{\infty}\int_{V_l^{N_l}}d\mathbf{r}^{N_l}f_{T,\mu,V_l}(\mathbf{r}^{N_l};N_l)\Bigg[\sum_{k=1}^{2}\sum_{i=1}^{N_l}x_i\overline{f_{x,i}^{[k]}}\Bigg]\\&=-\frac{1}{V_l}\Bigg\langle\sum_{k=1}^{2}\sum_{i=1}^{N_l}x_i\overline{f_{x,i}^{[k]}}\Bigg\rangle,\end{aligned} \tag{30}$$

$$T_{yy,FS}=0, \tag{31}$$

and

$$\begin{aligned}T_{zz,FS}&=-\frac{1}{V_l}\int_{V_l^{N_l}}d\mathbf{r}^{N_l}f_{T,\mu,V_l}(\mathbf{r}^{N_l};N_l)\Bigg[\sum_{k=1}^{2}\sum_{i=1}^{N_l}\left(z_i\pm\frac{s_z}{2}\right)\overline{f_{z,i}^{[k]}}\Bigg]\\&=-\frac{1}{V_l}\Bigg\langle\sum_{k=1}^{2}\sum_{i=1}^{N_l}\left(z_i\pm\frac{s_z}{2}\right)\overline{f_{z,i}^{[k]}}\Bigg\rangle.\end{aligned} \tag{32}$$

In Eqs. (30) and (32)

$$\overline{f_{\alpha,i}^{[k]}}:=-\frac{\partial\Phi^{[k]}(x_i,z_i;d_s,s_x,s_z)}{\partial\alpha_i},\quad\alpha=x,z \tag{33}$$

is the α component of the force exerted by wall k on film molecule i. The overbar is intended to stress the mean-field character of this force. In Eq. (31) $T_{yy,FS}$ vanishes identically because $\Phi^{[k]}$ is independent of y. Expressions for $\overline{f_{x,i}^{[k]}}$ and $\overline{f_{z,i}^{[k]}}$ can be obtained directly from Eq. (13) by a straightforward, albeit algebraically laborious, derivation. The results are given in Eqs. (A1) and (A3) of the Appendix for the sake of completeness.

A different expression for T_{zz} can be obtained directly from Eq. (24) without the transformation of coordinates. Therefore it is convenient to recast the configuration integral as [40]

$$Z_{N_l}=\int_{-s_z/2}^{s_z/2}dz_1 g_1, \tag{34}$$

where

$$g_1:=\int_{-s_x/2}^{s_x/2}dx_1\int_{-s_y/2}^{s_y/2}dy_1\prod_{i=2}^{N_l}\int_{-s_x/2}^{s_x/2}dx_i\times\int_{-s_y/2}^{s_y/2}dy_i\int_{-s_z/2}^{s_z/2}dz_i\exp[-\beta(U_{FF}+U_{FS})]. \tag{35}$$

By applying Leibniz's rule for the differentiation of an integral [41] it follows from Eqs. (22) and (34) that

$$\frac{\partial Z_{N_l}}{\partial s_z}=\int_{-s_z/2}^{s_z/2}dz_1\frac{\partial g_1}{\partial s_z}+\frac{1}{2}[g_1(z_1=s_z/2)+g_1(z_1=-s_z/2)]. \tag{36}$$

The last two terms in Eq. (36) can be written more explicitly as

$$\int_{-s_x/2}^{s_x/2}dx_1\int_{-s_y/2}^{s_y/2}dy_1\prod_{i=2}^{N_l}\int_{-s_x/2}^{s_x/2}dx_i\int_{-s_y/2}^{s_y/2}dy_i\int_{-s_z/2}^{s_z/2}dz_i\times\{\exp[-\beta U(x_1,y_1,z_1=s_z/2,x_2,\ldots,z_{N_l})]+\exp[-\beta U(x_1,y_1,z_1=-s_z/2,x_2,\ldots,z_{N_l})]\}=0 \tag{37}$$

because $\lim_{z_1\to\pm s_z/2}U_{FS}=\infty$, which is a consequence of the divergence of the function Δ [see Eqs. (9)–(13)] in that limit. Replacing g_1 by g_2, where g_2 is defined analogously to g_1, we may repeat the above argument N_l-1 times, to obtain finally

TABLE II. Normal component of the stress tensor $T_{zz}(s_z)$ from virial [Eqs. (28), (29)–(32)] and force [Eq. (38)] expressions for $\mu^*=-11.50$ and $\epsilon_{fs}^*=1.00$.

s_z^*	T_{zz}^* [Eq. (38)]	T_{zz}^* [Eq. (28)]	$T_{zz,FF}^*$	$T_{zz,FS}^*$
1.90	−2.251	−2.261	−0.112	−2.149
2.10	0.020	0.021	−0.140	0.161
2.20	0.341	0.339	−0.138	0.477
2.30	0.379	0.385	−0.136	0.521
2.50	0.227	0.232	−0.140	0.372
2.70	−0.043	−0.056	−0.195	0.139
3.00	−0.183	−0.177	−0.271	0.093
3.80	−0.040	−0.037	−0.187	0.150
4.50	0.052	0.055	−0.111	0.170
5.00	0.015	0.020	−0.120	0.141
10.00	−0.026	−0.028	−0.048	0.020

$$
\begin{aligned}
T_{zz} &= -A_z^{-1}\sum_{N_l=0}^{\infty}\int_{V_l^{N_l}} d\mathbf{r}^{N_l} f_{T,\mu,V_l}(\mathbf{r}^{N_l};N_l)\,\frac{\partial U_{FS}}{\partial s_z} \\
&= -A_z^{-1}\sum_{N_l=0}^{\infty}\int_{V_l^{N_l}} d\mathbf{r}^{N_l} f_{T,\mu,V_l}(\mathbf{r}^{N_l};N_l) \\
&\quad\times\sum_{k=1}^{2}\sum_{i=1}^{N_l}\frac{\partial\Phi^{[k]}(x_i,z_i;d_s,s,s_z)}{\partial s_z} \\
&= \frac{1}{2A_z}\sum_{N_l=0}^{\infty}\int_{V_l^{N_l}} d\mathbf{r}^{N_l} f_{T,\mu,V_l}(\mathbf{r}^{N_l};N_l)\sum_{i=1}^{N_l}[\overline{f}_{z,i}^{[1]}-\overline{f}_{z,i}^{[2]}] \\
&= \frac{\left\langle\sum_{i=1}^{N_l}[\overline{f}_{z,i}^{[1]}-\overline{f}_{z,i}^{[2]}]\right\rangle}{2A_z}.
\end{aligned}
\tag{38}
$$

Because $T_{\alpha\alpha}$ is clearly expressed as the average force exerted on (unit area of) the substrate, we refer to Eq. (38) as the ''force'' expression, whereas we term the previously derived form [Eqs. (28) and (29)–(32)] the ''virial'' expression. Force and virial expressions provide a useful check on the accuracy of the simulations because they invoke independent computational routes to the same physical quantity (see Table II).

B. Tensions

For a subsequent discussion of phase behavior in systems with interfaces, it is convenient to recast Eq. (18) in terms of certain ''tensions'' related to various components of **T** [42]. If the substrate is chemically homogeneous these (interfacial) tensions are related to the work associated with a change of the area of the fluid-substrate interface. For the present heterogeneous substrate a ''line'' tension may also be defined, which is a measure of the work required to alter the length of the line of fluid-substrate contact at which the two homogeneous portions of the substrate meet (see Fig. 1). Thus it is convenient to transform the extensive variables in Eq. (18) according to $\{s_x,s_y,s_z\}\rightarrow\{V_l,A_l,L_l\}$, where the length of the contact line is $L_l=4s_y$. The definition of A_l is somewhat less obvious. For instance, one may take $A_l=A_{\parallel}=2s_xs_y$ or, alternatively, $A_l=A_{\perp}=2s_zs_y$ as the relevant interfacial area [43]. However, in the limiting case of a chemically homogeneous substrate $A_{\perp}$ is not a physically relevant quantity. On the other hand, $A_{\parallel}$ remains physically meaningful because of the presence of the substrate, regardless of whether it is chemically structured or not. Thus we prefer the set of variables $\{V_l,A_{\parallel},L_l\}$ and rewrite Eq. (18) as

$$
dW=T_{zz}dV_l+\frac{s_z}{2}(T_{xx}-T_{zz})dA_{\parallel}+\frac{s_xs_z}{4}(T_{yy}-T_{xx})dL_l. \tag{39}
$$

In terms of the new variables Eq. (17) can be recast as

$$
d\Omega=-SdT-N_ld\mu+\gamma_Vdv_l+\gamma_{\parallel}dA_{\parallel}+\gamma_Ldl_l, \tag{40}
$$

where from Eqs. (17), (18), and (39) the tensions are given by

$$
\begin{aligned}
\gamma_V &= \left(\frac{\partial\Omega}{\partial V_l}\right)_{T,\mu,A_{\parallel},L_l}=T_{zz}, \\
\gamma_{\parallel} &= \left(\frac{\partial\Omega}{\partial A_{\parallel}}\right)_{T,\mu,V_l,L_l}=\frac{s_z}{2}(T_{xx}-T_{zz}), \\
\gamma_L &= \left(\frac{\partial\Omega}{\partial L_l}\right)_{T,\mu,V_l,A_{\parallel}}=\frac{s_xs_z}{4}(T_{yy}-T_{xx}).
\end{aligned}
\tag{41}
$$

From Eq. (40) we have

$$
\Omega=\gamma_VV_l+\gamma_{\parallel}A_{\parallel}+\gamma_Ll_l, \tag{42}
$$

which follows because Ω is a homogeneous function of degree one in s_y provided T,μ,s_x, and s_z are held constant. Note that Eq. (42) reduces to Eq. (19) through the relations given in Eq. (41).

As the separation between the substrates becomes very large, the diagonal elements of **T** must tend to the (negative) bulk pressure P_{bulk}. That is,

$$
\lim_{s_z\rightarrow\infty}T_{\alpha\alpha}=-P_{\text{bulk}}. \tag{43}
$$

Thus from Eqs. (19) and (41)–(43) we deduce

$$
\lim_{s_z\rightarrow\infty}\frac{\gamma_{\parallel}}{\gamma_L}=-\frac{2}{s_x}. \tag{44}
$$

C. Isothermal compressibility

Phase behavior is conveniently characterized by the average film density as well as by fluctuations of the density, which are reflected in the isothermal compressibility. To derive a molecular expression for the latter quantity we start from the Gibbs-Duhem relation

$$
\begin{aligned}
0 &= -SdT-N_ld\mu+(T_{xx}-T_{yy})A_xds_x+(T_{zz}-T_{yy})A_zds_z \\
&\quad -A_yd(s_yT_{yy}),
\end{aligned}
\tag{45}
$$

which results from combining Eqs. (17) and (19). Thus, fixing T, s_x, and s_z, we have

$$N_l d\mu = -A_y d(s_y T_{yy}). \tag{46}$$

If s_y is also fixed $\mu=\mu(N_l)$ and $T_{yy}=T_{yy}(N_l)$ and from Eq. (46) we deduce

$$N_l\left(\frac{\partial\mu}{\partial N_l}\right)_{T,s_x,s_y,s_z} = -\left(\frac{\partial(s_y A_y T_{yy})}{\partial N_l}\right)_{T,s_x,s_y,s_z}. \tag{47}$$

The right-hand side of Eq. (47) can be expressed alternatively as

$$\begin{aligned} -\left(\frac{\partial(s_y A_y T_{yy})}{\partial N_l}\right)_{T,s_x,s_y,s_z} &= -\left(\frac{\partial T_{yy}}{\partial(N_l/s_y A_y)}\right)_{T,s_x,s_y,s_z} \\ &= \frac{(s_y A_y)^2}{N_l}\left(\frac{\partial T_{yy}}{\partial(s_y A_y)}\right)_{T,s_x,N_l,s_z} \\ &= \frac{V_l}{N_l}\kappa_{yy}^{-1}, \end{aligned} \tag{48}$$

where the third line defines the isothermal compressibility κ_{yy}. From Eq. (17) we have

$$\left(\frac{\partial\Omega}{\partial\mu}\right)_{T,s_x,s_y,s_z} = -N_l \tag{49}$$

from which

$$\left(\frac{\partial^2\Omega}{\partial\mu^2}\right)_{T,s_x,s_y,s_z} = -\left(\frac{\partial N_l}{\partial\mu}\right)_{T,s_x,s_y,s_z} \tag{50}$$

immediately follows. Equations (20) and (21) yield

$$\begin{aligned} \left(\frac{\partial^2\Omega}{\partial\mu^2}\right)_{T,s_x,s_y,s_z} &= -\beta\Xi^{-1}\sum_{N_l=0}^{\infty} N_l^2 \frac{\exp[\beta\mu N_l]}{N_l!\Lambda^{3N_l}} Z_{N_l} \\ &\quad + \beta\left(\Xi^{-1}\sum_{N_l=0}^{\infty} N_l \frac{\exp[\beta\mu N_l]}{N_l!\Lambda^{3N_l}} Z_{N_l}\right)^2 \\ &= -\beta(\langle N_l^2\rangle - \langle N_l\rangle^2). \end{aligned} \tag{51}$$

The desired molecular expression for κ_{yy} results finally from combining Eqs. (47), (48), (50), and (51) to get

$$\kappa_{yy} = \beta V_l \frac{\langle N_l^2\rangle - \langle N_l\rangle^2}{\langle N_l\rangle^2}. \tag{52}$$

Before turning to a discussion of the results, we emphasize that the lamella is a virtual construct introduced to distinguish precisely between the *system* and its *environment* in a thermodynamic sense. The lamella could in principle constitute *any* piece of the film. Henceforth, we take the lamella to coincide with the computational cell, setting $N_f=N_l$, $V=V_l=s_x s_y s_z$, and $L=L_l=4s_y$.

IV. RESULTS

Symbols with asterisks refer to reduced variables, which are unitless. The dimensionless units are based on the parameters of the LJ(12,6) potential for the film-film interaction:

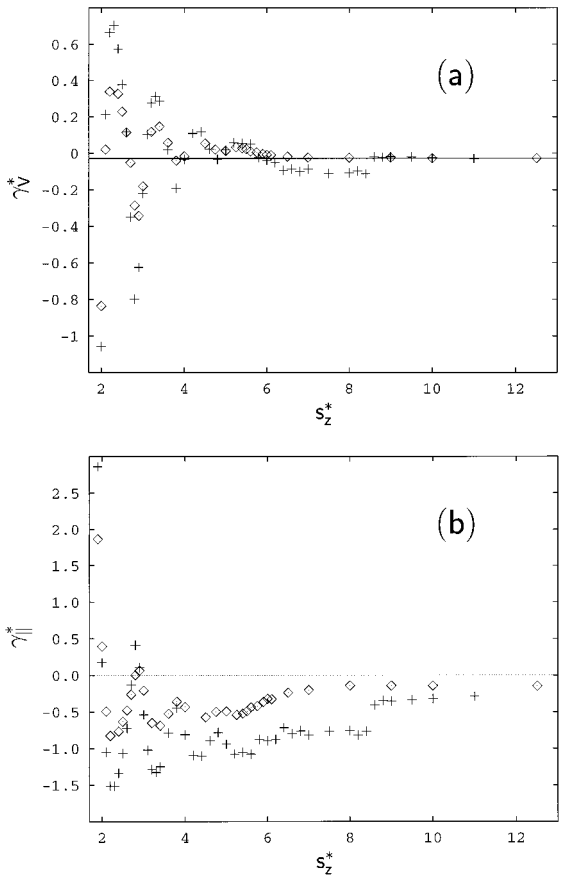

FIG. 2. (a) Volume tension γ_V^* as a function of substrate separation s_z^*; ($\diamond$) $\epsilon_{fs}^*=1.00$, (+) $\epsilon_{fs}^*=1.25$. The horizontal solid line corresponds to $\lim_{s_z\to\infty} T_{zz}^* = -P_{\rm bulk}^* = -0.029$. (b) Same as (a) but for areal tension $\gamma_\parallel^*$.

distance is given in units of σ; energy in units of ϵ_{ff}; temperature in units of $\epsilon_{ff}k_B^{-1}$. Everywhere in this paper numerical values are given in dimensionless units. In the remainder of this paper we fix the following substrate parameters: $s_x^*=10.0$, $d_s^*=4.0$, $\epsilon_{fw}^*=10^{-3}$. Two different strengths of interaction of the strongly adsorbing central strip with film molecules are employed, these being specified by $\epsilon_{fs}^*=1.00$ and 1.25. We also fix $T^*=1.00$ and $\mu^*=-11.5$, for which the Lennard-Jones bulk phase is a gas with a(n average) number density $\overline{n_{\rm bulk}^*}=\langle N\rangle/V^*=0.036$.

A. Tensions and stratification

The various ''tensions'' introduced in Sec. III B are plotted as functions of s_z in Figs. 2 and 3. For $\epsilon_{fs}^*=1.00$ and 1.25 the volume tension γ_V in Fig. 2 is a damped oscillatory function of substrate separation as in the case of a Lennard-Jones fluid between chemically homogeneous substrates [11,22]. Regardless of the value of ϵ_{fs}^*, γ_V reaches its limiting value $-P_{\rm bulk}^*=-0.029$ [see Eq. (43)] within the range of substrate separations studied. Changes of ϵ_{fs}^* affect only the amplitude of the oscillations of γ_V; peak positions are largely unaltered. Oscillations of γ_V are ''fingerprints'' of stratification, that is, the tendency of film molecules to arrange themselves in individual strata parallel with the walls [21,22]. Stratification is due to geometric constraints on the packing of spheri-

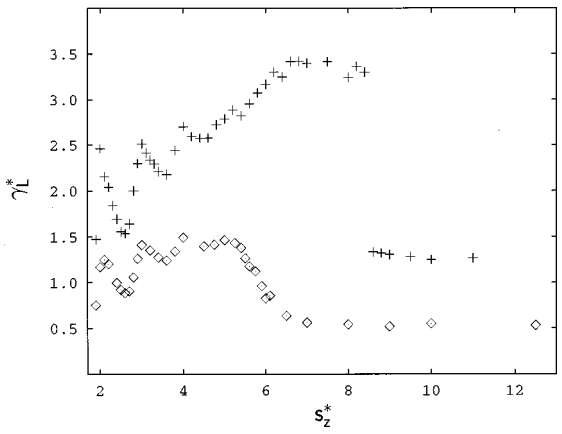

FIG. 3. Same as Fig. 2, but for line tension γ_L^*.

cal molecules between planar substrates. Because peak positions are essentially determined by these geometric constraints, one does not expect the structure of $\gamma_V(s_z)$ to depend significantly on ϵ_{fs}^*. Thus it is not surprising that neighboring peaks of γ_V are separated by a distance $\Delta s_z^* \simeq 1$, regardless of ϵ_{fs}^*.

In the chemically striped pore, however, the film is stratified only over the attractive central strip of the substrate, as can be seen in Fig. 4 where we plot the local density

$$\rho^{[1]}(x,z;d_s,s_x,s_z)=\frac{\langle N(x,z;d_s,s_x,s_z)\rangle}{\Delta x \Delta z s_y}, \tag{53}$$

where $\langle N(x,z;d_s,s_x,s_z)\rangle$ is the average number of film molecules whose centers are contained by the square prism of dimensions $\Delta x \times \Delta z \times s_y$ centered on (x,z) with $\Delta x^* = \Delta z^* = 0.05$. Since $\rho^{[1]}$ must be symmetric about the $x=0$ and $z=0$ planes, the plot shows only the upper right quadrant of the x-z plane. Peaks in $\rho^{[1]}(x,z;d_s,s_x,s_z)$ represent positions of molecular strata. The plot also indicates that stratification diminishes over the central strip as the distance from the substrate increases and that it is absent over the repulsive, nonwetted outer strips. Thus for the substrate separation on which Fig. 4 is based a stratified ''liquid'' bridges the gap between the central strips of the two opposite substrates and is surrounded by a nearly homogeneous gas phase.

Stratification is also reflected in the areal tension $\gamma_\parallel$ plotted in Fig. 2(b) for the two values of ϵ_{fs}^*. However, maxima

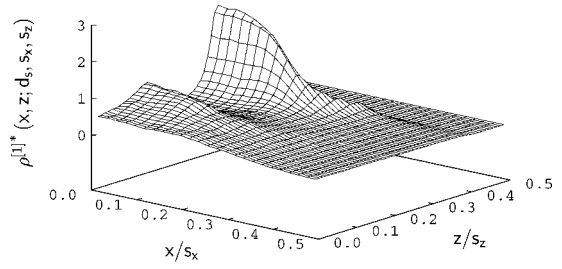

FIG. 4. Local density $\rho^{[1]*}(x,z;d_s,s_x,s_z)$ as a function of x/s_x and z/s_z for $s_z^*=5.40$. Film-substrate interface is located at $z/s_z=0.5$ with the wetted (central) and the nonwetted (outer) strips ranging from $0.0 \leqslant x/s_x \leqslant 0.2$ and from $0.2 < x/s_x \leqslant 0.5$, respectively. The plot is symmetric with respect to the planes $x=0$ and $z=0$.

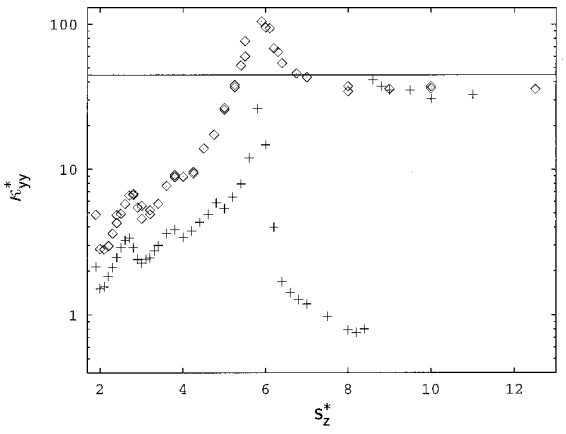

FIG. 5. Isothermal compressibility κ_{yy}^* as a function of substrate separation s_z^*. ($\diamond$) $\epsilon_{fs}^*=1.00$, (+) $\epsilon_{fs}^*=1.25$. The horizontal solid line represents the isothermal compressibility of the Lennard-Jones bulk phase at $T^*=1.00$ and $\mu^*=-11.50$.

in $\gamma_\parallel$ are out of phase by about half a period of the oscillation compared with γ_V. Although $\gamma_\parallel$ seems to oscillate around a constant value of approximately $-0.5(\epsilon_{fs}^*=1.00)$ and $-0.9(\epsilon_{fs}^*=1.25)$ for substrate separations ($s_z^* \lesssim 5.0$) where stratification is evident in the plots of γ_V [cf. Fig. 2(a)], a significant increase of $\gamma_\parallel$ is observed at larger substrate separations of $5.2 < s_z^* < 6.0$ ($\epsilon_{fs}^*=1.00$) and $s_z^* \simeq 8.5$ ($\epsilon_{fs}^*=1.25$). This variation of $\gamma_\parallel$ is also reflected in a parallel plot of γ_L in Fig. 3, which suggests a marked dependence of the film's behavior on ϵ_{fs}^*. For example, for $\epsilon_{fs}^*=1.00$ the line tension decreases continuously over the range $5.2 < s_z^* < 6.0$ whereas for $\epsilon_{fs}^*=1.25$ it first rises to a plateau and then drops discontinuously at $s_z^* \simeq 8.5$. These variations are mirrored by $\gamma_\parallel$, albeit rather dully, which suggests that γ_L is the more sensitive indicator of structural transformations accompanying changes in the substrate separation.

Note that the ratio $\gamma_L^*/\gamma_\parallel^* = -0.28$ for $s_z^*=12.5$ ($\epsilon_{fs}^*=1.00$) and $\gamma_L^*/\gamma_\parallel^* = -0.23$ for $s_z^*=11.0$ ($\epsilon_{fs}^*=1.25$) which is close to the theoretical value of -0.2 for $s_x^*=10.0$ in the large-system limit [see Eq. (44)]. Thus, for the largest substrate separations studied, the film may be viewed crudely as a bulk phase, in spite of the nonvanishing tensions $\gamma_\parallel$ and γ_L. They signal an anisotropy in the film caused by the heterogeneity of the substrate, which persists indefinitely (i.e., as $s_z \to \infty$).

B. Phase behavior

The isothermal compressibility κ_{yy} is plotted in Fig. 5 as a function of s_z for $\epsilon_{fs}^*=1.00$ and 1.25. In both cases $\kappa_{yy}(s_z)$ increases up to $s_z^* \simeq 6.0$. The compressibility for $\epsilon_{fs}^*=1.25$ is smaller than for $\epsilon_{fs}^*=1.00$, indicating that the film is denser for the more attractive central strip, as would be expected. The nonmonotonic dependence of κ_{yy} on $s_z(s_z^*<6.0)$ signifies stratification of the film over the central strip (see Fig. 4) [21,22]. In the vicinity of $s_z^*=5.6$ both compressibility curves exhibit a large maximum. However, the curve for $\epsilon_{fs}^*=1.00$ decays monotonously to a value close to the bulk compressibility $\kappa_T^{\text{bulk}*}=44.60$ for all $s_z^* \geqslant 6.0$, while the curve for $\epsilon_{fs}^*=1.25$ approaches a much smaller value over

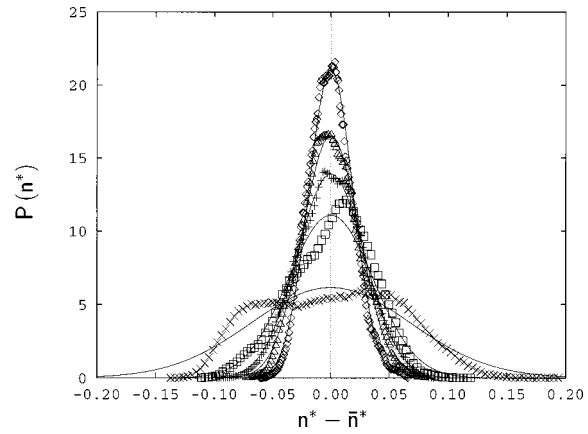

FIG. 6. Normalized density distribution $P(n^*)$ for various values of s_y^* ; (X) $s_y^*=10$, (□) $s_y^*=30$, (+) $s_y^*=50$, (△) $s_y^*=65$, (◇) $s_y^*=100$. Solid lines represent a fit of a Gaussian to $P(n)$.

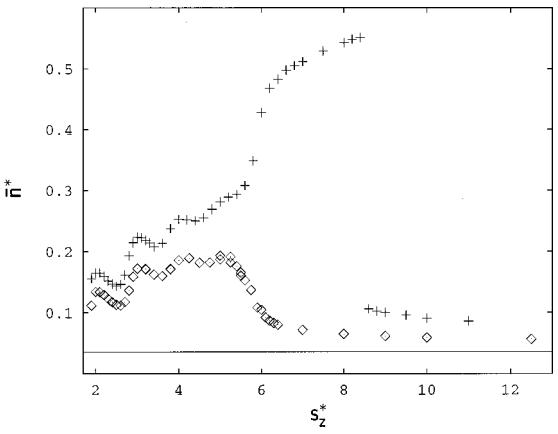

FIG. 7. Same as Fig. 5, but for the film average density $\overline{n^*}$. The solid horizontal line corresponds to the bulk density $\overline{n^*_{\rm bulk}}=0.036$.

the range $6.0\leqslant s_z^*<8.4$ corresponding to typical compressibilities of a dense Lennard-Jones liquid. Between $8.4<s_z^*<8.6$ the compressibility for $\epsilon_{fs}^*=1.25$ rises discontinuously to the same bulklike value observed for $\epsilon_{fs}^*=1.00$.

We note that regardless of the value of ϵ_{fs}^*, κ_{yy} depends significantly on the size of the computational cell in the vicinity of its first maximum. This is illustrated in Fig. 6, which displays density distributions $P(n)$ for various values of s_y, $\epsilon_{fs}^*=1.25$, and $s_z^*=5.60$, where $n:=N_f/V$. For a sufficiently large system $P(n)$ should be roughly a Gaussian centered at the most probable density $\tilde{n}$ [37]. It is easy to verify that the standard deviation σ_n of $P(n)$ in the Gaussian limit is related to κ_{yy} via [37]

$$\sigma_n=\overline{n}\sqrt{\frac{k_BT}{A_y}\kappa_{yy}s_y^{-1/2}}, \tag{54}$$

where $\overline{n}:=\langle N_f\rangle/V$. Likewise the height of the peak $P(\tilde{n})$ is proportional to $\sqrt{s_y}$. If $s_y^*=10$ the plot in Fig. 6 shows that the density distribution is not Gaussian but rather bimodal, indicating that the system ''oscillates'' between high- and low-density states. As s_y increases the bimodal nature of $P(n)$ gradually declines and for $s_y^*\geqslant 50.0$, $P(n)$ is Gaussian with the required dependence of peak height and standard deviation on s_y. Thus, if we fit the theoretical expression $P(n)=(\sqrt{2\pi}\sigma_n)^{-1}\exp[-(n-\overline{n})^2/2\sigma_n^2]$ to the curves shown in Fig. 6, taking σ_n as a parameter with $\overline{n}=\langle N_f\rangle/A_ys_y=$const at fixed A_y, κ_{yy} is obtained from the slope of the straight line $\sigma_n=f(s_y^{-1/2})$ through the origin ($s_y^*\geqslant 50.0$). Data in the vicinity of the peaks of $\kappa_{yy}(s_z)$ plotted in Fig. 5 are obtained by this procedure. However, for $\epsilon_{fs}^*=1.00$ a small range $5.6\leqslant s_z^*\leqslant 6.0$ remains where the bimodal nature of $P(n)$ does not vanish completely even for $s_y^*=250$, although a clear but gradual tendency toward a Gaussian is observed over the range $100\leqslant s_y^*\leqslant 250$. Consequently, we refrain from plotting κ_{yy} in Fig. 5 for $\epsilon_{fs}^*=1.00$ in the range $5.6\leqslant s_z^*\leqslant 6.0$. However, we should also point out that no such system-size dependence is detected for other quantities such as **T** and $\overline{n}$.

Additional light can be thrown on the nature of the phase transformations responsible for variations in κ_{yy} by an examination of the dependence of the mean density $\overline{n}$ on s_z (see Fig. 7). In concordance with the tensions (Figs. 2 and 3) and the local density (Fig. 4), $\overline{n(s_z)}$ is an oscillatory function over the range of substrate separations where the film is stratified (Fig. 4). In the vicinity of the maximum of $\kappa_{yy}(s_z)$, however, $\overline{n(s_z)}$ shows a pronounced increase for $\epsilon_{fs}^*=1.25$ and a similarly strong decrease for $\epsilon_{fs}^*=1.00$. The discontinuous change of $\overline{n(s_z)}$ around $s_z^*\simeq 8.5$ for $\epsilon_{fs}^*=1.25$ can be interpreted as capillary condensation (or evaporation), that is, as a first-order phase transition analogous to condensation or evaporation of a subcritical bulk fluid. Ancillary plots show that for $s_z^*>6.0$ ($\epsilon_{fs}^*=1.00$) and $s_z^*>8.5$ ($\epsilon_{fs}^*=1.25$) $\overline{n(s_z)}\propto s_z^{-1}$. In Sec. IV C it is shown that for these ranges of s_z^* the liquid bridge has collapsed, leaving ''nanodroplets'' on the central strips in equilibrium with dilute gas. As s_z increases, the nanodroplets do not change. Hence $\langle N_f(s_z)\rangle$ remains approximately constant and $\overline{n(s_z)}$ decays as s_z^{-1}.

For $\epsilon_{fs}^*=1.25$ and s_z^* in the range 5.8–8.4, a plot of $\overline{n(s_z)}$ versus s_z can be well fitted by the expression

$$\overline{n(s_z)}=a+bs_z^{-1}. \tag{55}$$

In this range of s_z the stratified structure of the liquid bridge in the immediate vicinity of the substrates has been established and new molecules are added to the homogeneous inner portion of the bridge, whose density, given by

$$\overline{n}_{\rm inner}=\frac{\langle N(s_z)\rangle-\langle N_{\rm strata}\rangle}{A_\parallel(s_z-\delta)}=\frac{\overline{n(s_z)}}{1-\delta/s_z}-\frac{\delta\overline{n}_{\rm strata}}{s_z(1-\delta/s_z)}, \tag{56}$$

remains approximately *constant*. In Eq. (56) δ stands for the thickness of the stratified part of the film and $\overline{n}_{\rm strata}=\langle N_{\rm strata}\rangle/\delta A_\parallel$ for its mean density, which we assume to be constant. Rearrangement of Eq. (56) yields Eq. (55) with the correspondences

$$a=\overline{n}_{\rm inner},$$

$$b=-\delta(\overline{n}_{\rm inner}-\overline{n}_{\rm strata}). \tag{57}$$

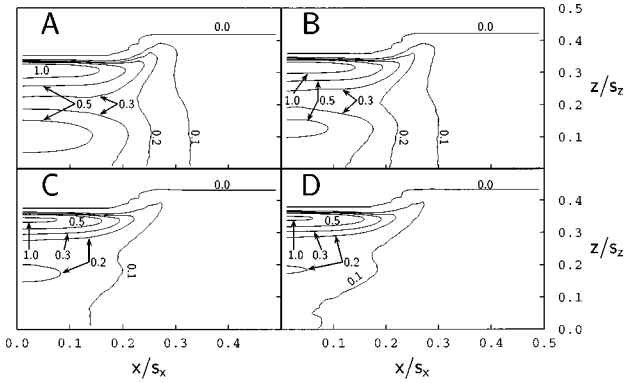

FIG. 8. Contour maps of local density $\rho^{[1]}(x,z;d_s,s_x,s_z)$ for $\epsilon_{fs}^*=1.00$ and substrate separations of $s_z^*=5.25$ (A), 5.50 (B), 6.00 (C), and 6.40 (D). Solid lines connect points (x,z) corresponding to $\rho^{[1]*}(x,z;d_s,s_x,s_z)=c$, where values of constant c are indicated by arrows.

Finally, the maximum in $\kappa_{yy}(s_z)$ and the discontinuity for $\epsilon_{fs}^*=1.25$ are unique features due to the chemical heterogeneity of the substrate. As we demonstrate elsewhere [44], neither the maximum nor the discontinuity occurs for the chemically homogeneous substrate composed entirely of either ''weak'' (i.e., $d_s=0$) or ''strong'' (i.e., $d_s=s_x$, $f=1.25$) species.

C. Microscopic structure

Variations of $\overline{n}$, κ_{yy}, γ_L, $\gamma_\parallel$, and γ_V are accompanied by changes in the film's microscopic structure, which can be visualized by contour maps of the local density $\rho^{[1]}(x,z;d_s,s_x,s_z)$ [see Eq. (53), Fig. 4] shown in Figs. 8 and 9. On account of the symmetry of the system, contours are plotted only in the upper right quadrant of the x-z plane. For $\epsilon_{fs}^*=1.00$ and $s_z^*=5.25$ Fig. 8(A) shows that the fluid is stratified over the central strip ($x/s_x\leqslant 0.2$) and that the strata become less distinct as their distance from the substrate increases. A comparison with Fig. 5 shows that the substrate separation for Fig. 8(A) is smaller than the one where $\kappa_{yy}(s_z)$ assumes its maximum. Along a path $x/s_x=0.0$ to 0.5, the density $\rho^{[1]}(x,z=0;d_s,s_x,s_z)$ decreases steadily. Thus the film consists of a liquidlike ''bridge,'' stabilized by opposing strong central strips of the two substrates and surrounded by a low-density gas. The interface between the bridge and the gas can be described in terms of a phenomenological model usually applied to the planar interface between coexisting bulk liquid and gas phases [45]. The nature of the interface between the bridge and the gas is detailed in [44].

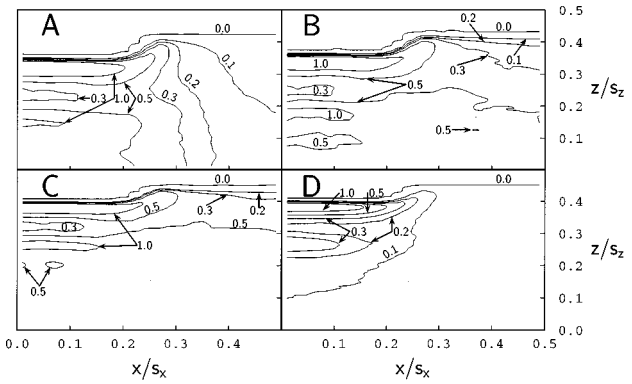

FIG. 9. Same as Fig. 8, but for $\epsilon_{fs}^*=1.25$ and substrate separations of $s_z^*=5.40$ (A), 6.20 (B), 8.40 (C), and 8.60 (D).

As s_z approaches the maximum of $\kappa_{yy}(s_z)$ more closely the bridge disappears gradually. For example, at $s_z^*=5.50$ [Fig. 8(B)] intersections of contour lines corresponding to $\rho^{[1]*}(x,z;d_s,s_x,s_z)=0.1$, 0.2, and 0.3 with the x axis are shifted to smaller values of x/s_x and stratification is less pronounced. The latter is particularly evident from the contour $\rho^{[1]*}(x,z;d_s,s_x,s_z)=0.5$ located approximately at $z/s_z\approx 0.1$, which encloses a region in the x-z plane smaller at $s_z^*=5.50$ than at $s_z^*=5.25$. Thus the interface between the bridge and the gas phase forms a nanoscopic meniscus.

As s_z passes through the maximum in $\kappa_{yy}(s_z)$ (see Fig. 5) this tendency persists. For example, for $s_z^*=6.00$ [Fig. 8(C)] the liquid-gas interface is no longer observed. Note also that the contour $\rho^{[1]*}(x,z;d_s,s_x,s_z)=0.1$ intersects the x axis at increasingly smaller values of x/s_x over the range $5.25\leqslant s_z^*\leqslant 6.40$. The contour maps for $s_z^*=6.00$ and 6.40 [Fig. 8(D)] reveal that the bridge has given way to nanodroplets localized on the central strips of each substrate. However, the interaction of film molecules with this part of the substrate is so weak that the nanodroplets remain diffuse, as indicated by the contour $\rho^{[1]*}(x,z;d_s,s_x,s_z)=0.1$, which still intersects the x axis at $s_z^*=6.40$.

For $\epsilon_{fs}^*=1.25$ the maximum of $\kappa_{yy}(s_z)$ corresponds to an entirely different process, which is evident from the plots in Figs. 9(A) and 9(B), where the contour maps of $\rho^{[1]}(x,z;d_s,s_x,s_z)$ are shown for $s_z^*=5.40$ and $s_z^*=6.20$ (cf. Fig. 5). For $s_z^*=5.40$ the liquid bridge is reflected by the contours $\rho^{[1]*}(x,z;d_s,s_x,s_z)=0.20$, 0.30, and 0.50 which intersect the x axis [see Fig. 9(A)]. This situation is similar to the one depicted for $\epsilon_{fs}^*=1.00$ in Figs. 8(A) and 8(B). However, now the surrounding gas is at higher density because the contour $\rho^{[1]*}(x,z;d_s,s_x,s_z)=0.10$ does not intersect the x axis as in the case of $\epsilon_{fs}^*=1.00$ [see Figs. 8(A) and 8(B)]. As s_z passes through the maximum of $\kappa_{yy}(s_z)$ (see Fig. 5) the interface vanishes completely. The contours in Fig. 9(B) now run parallel with the x axis (and therefore parallel with the substrate located at $z/s_z=0.5$), indicating that the liquid bridge induces some sort of ''condensation'' of the surrounding gas phase beyond some critical substrate separation. However, according to the plot of $\overline{n}(s_z)$ in Fig. 7, in conjunction with the system-size dependence of $P(n)$ (see Fig. 6) this ''condensation'' does not seem to be an ordinary first-order phase transition. Rather it appears to be a continuous process during which the liquid bridge alone stabilizes a fluid phase which is otherwise not supported by the nonwetted (i.e., purely repulsive) strip of the substrate.

As s_z^* increases beyond 6.2 [see Fig. 9(C)] the fluid phase in the vicinity of the nonwetted strips becomes more stable, as can be seen particularly from the contour $\rho^{[1]*}(x,z;d_s,s_x,s_z)=0.5$, which is not only more nearly parallel with the x axis than in Fig. 9(B), but also closer to the substrate located at $z/s_z=0.5$. Finally, a comparison of Figs. 5 and 7 with Figs. 9(C) and 9(D) shows that the dis-

continuity in $\overline{n(s_z)}$ and $\kappa_{yy}(s_z)$ at $s_z^* \simeq 8.50$ corresponds to a first-order phase transition during which the fluid evaporates, leaving behind again nanodroplets which are stabilized entirely by the central wetted strip. Formation of nanodroplets is signaled in particular by the contour corresponding to $\rho^{[1]*}(x,z;d_s,s_x,s_z)=0.10$, which bends backward to the z axis, enclosing all contours corresponding to higher values of $\rho^{[1]}(x,z;d_s,s_x,s_z)$. Because of the stronger interaction between the film and the central strip the nanodroplet is better defined than that observed in Figs. 8(C) and 8(D).

V. SUMMARY AND CONCLUSIONS

In this article we investigated the behavior of a Lennard-Jones film confined between two chemically heterogeneous substrates forming a slit-shaped nanopore. The substrate is modeled as a periodic sequence of strongly adsorbing slabs (of width d_s) alternating with weakly adsorbing ones (of width d_w). The thermodynamic state of the film is characterized by the (reduced) variables T^*, μ^*, s_z^*, d_s^*, d_w^*, ϵ_{fs}^*, and ϵ_{fw}^*. We fixed $T^*=1.00$, $\mu^*=-11.50$, $d_s^*=4.00$, $d_w^*=6.00$, and $\epsilon_{fw}^*=0.001$ and examined the dependence of the stresses, density, and isothermal compressibility on s_z^* for two values of ϵ_{fs}^* (1.00 and 1.25), which measures the attraction of film molecules for the strong strip relative to their mutual attraction. The greater ϵ_{fs}^* is, the stronger the attraction is. Our findings can be summarized as follows.

(1) Molecularly thin films between chemically heterogeneous substrates are stratified (see Fig. 4). However, stratification is observed only between the ''strong'' strips of the two opposite substrates, so that a liquid ''bridge'' exists in thermodynamic equilibrium with a surrounding gas phase stabilized by the ''weak'' strips.

(2) On account of stratification, tensions (see Figs. 2 and 3) and mean density (see Fig. 7) oscillate as functions of s_z with a period of approximately one ''diameter'' of the film molecule. This behavior is qualitatively similar to that observed for a Lennard-Jones film confined between chemically homogeneous ''strong'' substrates [44].

(3) A nonmonotonic increase and a maximum in $\kappa_{yy}(s_z)$ (see Fig. 5), which are not observed for a Lennard-Jones film confined by chemically homogeneous substrates [44], are due to the chemical heterogeneity of the substrate. The location of the maximum is nearly independent of ϵ_{fs}^*. However, a comparison with $\gamma_L(s_z)$ (Fig. 3) and $\overline{n(s_z)}$ (Fig. 7) shows that the maximum of $\kappa_{yy}(s_z)$ corresponds to different processes, depending on the value of ϵ_{fs}^*. The microscopic structure of the film, as revealed by contour maps of $\rho^{[1]}\times(x,z;d_s,s_x,s_z)$, shows that the maximum of $\kappa_{yy}(s_z)$ corresponds to the formation of ''nanodroplets'' stabilized by the ''strong'' strips of the substrate for $\epsilon_{fs}^*=1.00$ and to the formation of a dense fluid phase over the whole substrate for $\epsilon_{fs}^*=1.25$ (Figs. 8 and 9). Both processes result from a competition between the strong and ''weak'' strips of the heterogeneous substrate.

(4) Formation of a dense fluid phase over the whole substrate is a continuous process as inferred from the continuous variation of $n(s_z)$ in the neighborhood of the maximum in $\kappa_{yy}(s_z)$ (Figs. 5 and 7). The pronounced system-size dependence of $P(n)$ (Fig. 6) supports this notion.

(5) At larger separations for $\epsilon_{fs}^*=1.25$ the substrate cannot stabilize the liquidlike film, which evaporates. The transition is first order, as indicated by discontinuities in γ_L, κ_{yy}, and $\overline{n}$ (Figs. 3, 5, and 7) and leaves behind ''nanodroplets'' adhering to the ''strong'' strips (Fig. 9).

These results suggest the complex behavior to be expected for the simplest sort of fluid films confined by substrates possessing the simplest sort of chemical heterogeneity. We have superficially explored the dependence of this behavior on only one (ϵ_{fs}^*) of the *seven* thermodynamic state variables. We expect that variations in the ratios d_s/d_w and $\epsilon_{fs}/\epsilon_{fw}$ would have similarly marked influences on the film's behavior.

An intriguing question beyond the scope of the current study is the behavior of the film under shear. Shear strain can be measured in terms of the relative displacement of the two substrates in the x direction. The shear stress T_{zx} is the average x component of the force exerted by the film on unit interfacial area of the substrate [40]. It would be interesting to compare thin films sheared between atomically smooth, but chemically nanostructured, substrates with films between substrates composed of discrete atoms of one species, so that the substrate is smooth on a nanoscale, a situation which has been studied extensively [16,20,21,40,46]. The ability of a film between chemically heterogeneous, but infinitesimally smooth, substrates to sustain a nonvanishing shear stress likely depends on the strength of the interaction between film molecules and the strong strips of the substrate. On the other hand, for substrates that are structured on the atomic scale, but smooth on the nanoscale the influence of film-substrate attraction on shearing is known to be minor [40,46]; the constraints due to packing of film molecules between structured substrates dictate the shearing behavior.

Finally, we draw attention to the interesting question of the critical behavior of thin films confined by chemically heterogeneous substrates. Near the critical point the correlation length among film molecules can be of the order of the distance between the substrates. As a consequence the critical point of the film is shifted to lower temperature compared with the bulk phase. This effect, predicted by Nakanishi and Fisher [47] on the basis of a lattice-gas model, has also been observed in an experimental study [48] of adsorption of SF_6 in controlled-pore glasses and in a recent computer simulation [49] of a Lennard-Jones film in mesoscopic model slit-shaped pores composed of chemically homogeneous substrates. In [49] the depression of the critical temperature is correlated with variations of the microscopic structure of the fluid. In the case of chemically striped substrates it would be interesting to study the liquid bridge-vapor interface in the neighborhood of the bulk critical point.

ACKNOWLEDGMENTS

M.S. is grateful to the Deutsche Forschungsgemeinschaft (DFG) for financial support. D.J.D. acknowledges the support of the Office of Naval Research and the National Science Foundation. Both authors are grateful to the North Atlantic Treaty Organization whose support has facilitated their

collaboration. Computations were carried out on the Cray Y-MP of the Höchstleistungsrechenzentrum (HLRZ) at Forschungszentrum Jülich.

APPENDIX: FILM-SUBSTRATE FORCES

Here we present explicit formulas for the components $\overline{f_x^{[k]}}$ and $\overline{f_z^{[k]}}$ of the forces exerted by the substrate on a film molecule located at a point (x,z). Starting from the mean-field representation of the film-substrate potential given in Eq. (13) one has after tedious but straightforward algebra

$$\overline{f_x^{[k]}} = -\frac{\partial \Phi^{[k]}}{\partial x} = \frac{3\pi}{2} n_A \sigma^2 \sum_{m=-\infty}^{\infty} \sum_{m'=0}^{\infty} \times \left\{ (\epsilon_{fw}-\epsilon_{fs}) \chi\left(x+\frac{d_s}{2}-ms_x,\ \frac{s_z}{2}+m'\delta_{\diagup}\pm z \right) - (\epsilon_{fw}-\epsilon_{fs}) \chi\left(x-\frac{d_s}{2}-ms_x,\ \frac{s_z}{2}+m'\delta_{\diagup}\pm z \right) - \epsilon_{fw}\left[\chi\left(x+\frac{s}{2}-ms_x,\ \frac{s_z}{2}+m'\delta_{\diagup}\pm z \right) - \chi\left(x-\frac{s}{2}-ms_x,\ \frac{s_z}{2}+m'\delta_{\diagup}\pm z \right) \right] \right\}, \tag{A1}$$

where the function χ is defined by

$$\chi(x'',z'') = I_1(x'',z'') - I_2(x'',z'') \tag{A2}$$

and I_1 and I_2 are defined by Eqs. (6) and (7). The $\pm$ sign in the second argument of χ in Eq. (A1) is introduced to distinguish between the lower ($+$, $k=1$) and the upper ($-$, $k=2$) substrate, respectively. Similarly, one obtains

$$\overline{f_z^{[k]}} = -\frac{\partial \Phi^{[k]}}{\partial z} = \frac{3\pi}{2} n_A \sigma^2 \sum_{m=-\infty}^{\infty} \sum_{m'=0}^{\infty} \times \left\{ (\epsilon_{fw}-\epsilon_{fs}) \psi\left(x+\frac{d_s}{2}-ms_x,\ \frac{s_z}{2}+m'\delta_{\diagup}\pm z \right) - (\epsilon_{fw}-\epsilon_{fs}) \psi\left(x-\frac{d_s}{2}-ms_x,\ \frac{s_z}{2}+m'\delta_{\diagup}\pm z \right) - \epsilon_{fw}\left[\psi\left(x+\frac{s}{2}-ms_x,\ \frac{s_z}{2}+m'\delta_{\diagup}\pm z \right) - \psi\left(x-\frac{s}{2}-ms_x,\ \frac{s_z}{2}+m'\delta_{\diagup}\pm z \right) \right] \right\}, \tag{A3}$$

where

$$\psi(x'',z'';d_s,s_x,s_z) = \frac{21}{32} K_3(x'',z'';d_s,s_x,s_z) - K_4(x'',z'';d_s,s_x,s_z), \tag{A4}$$

$$K_3(x'',z'';d_s,s_x,s_z) = -\frac{2}{9}\frac{x''\sigma^{11}}{z''^3\sqrt{R^9}}\left[1+\frac{8}{7}S+\frac{48}{35}S^2+\frac{64}{35}S^3+\frac{128}{35}S^4 \right] - \frac{x''\sigma^{11}}{z''\sqrt{R^{11}}}\left[1+\frac{8}{7}S+\frac{48}{35}S^2+\frac{64}{35}S^3+\frac{128}{35}S^4 \right] - \frac{2}{9}\frac{x''^3\sigma^{11}}{z''^5\sqrt{R^9}}\left[\frac{8}{7}+\frac{96}{35}S+\frac{192}{35}S^2+\frac{512}{35}S^3 \right], \tag{A5}$$

$$K_4(x'',z'';d_s,s_x,s_z) = -\frac{2}{3}\frac{x''\sigma^5}{z''^3\sqrt{R^3}}(1+2S) - \frac{x''\sigma^5}{z''\sqrt{R^5}}(1+2S) - \frac{4}{3}\frac{x''^3\sigma^5}{z''^5\sqrt{R^3}}. \tag{A6}$$

The quantity S in Eqs. (A5) and (A6) is defined by Eq. (11).

[1] R. E. Grim, *Clay Mineralogy* (McGraw-Hill, New York, 1953), Chap. 8.

[2] P. F. Low, Langmuir **3**, 18 (1987).

[3] D. W. Thompson, *On Growth and Form* (Dover, New York, 1992), Chap. 5.

[4] B. Bhushan, J. N. Israelachvili, and U. Landman, Nature (London) **374**, 607 (1995).

[5] T. A. Core, W. K. Tsang, and S. J. Sherman, Solid State Technol. **36**, 39 (1993).

[6] D. Tabor and R. H. S. Winterton, Proc. R. Soc. London, Ser. A **312**, 435 (1969).

[7] S. Granick, Science **253**, 1374 (1991).

[8] J. N. Israelachvili, *Intermolecular and Surface Forces* (Academic, London, 1992).

[9] I. K. Snook and W. van Megen, J. Chem. Phys. **72**, 2907 (1980).

[10] D. Nicholson and N. G. Parsonage, *Computer Simulation and the Statistical Mechanics of Adsorption* (Academic, London, 1982).

[11] M. Schoen, *Computer Simulation of Condensed Phases in Complex Geometries* (Springer, Heidelberg, 1993).

[12] J. E. Curry, F. Zhang, J. H. Cushman, M. Schoen, and D. J. Diestler, J. Chem. Phys. **101**, 10824 (1994).

[13] M. Schoen and S. Dietrich, Phys. Rev. E **56**, 499 (1997).

[14] J. N. Israelachvili, Acc. Chem. Res. **20**, 415 (1987).
[15] J. N. Israelachvili and P. M. McGuiggan, Science **241**, 795 (1988).
[16] P. Bordarier, B. Rousseau, and A. H. Fuchs, J. Chem. Phys. **106**, 7295 (1997).
[17] L. A. Rowley, D. Nicholson, and N. G. Parsonage, Mol. Phys. **31**, 365 (1976).
[18] J. E. Lane and T. H. Spurling, Aust. J. Chem. **29**, 2103 (1980).
[19] M. Schoen, D. J. Diestler, and J. H. Cushman, J. Chem. Phys. **87**, 5464 (1987).
[20] M. Schoen, D. J. Diestler, and J. H. Cushman, Science **262**, 545 (1993).
[21] M. Schoen, D. J. Diestler, and J. H. Cushman, J. Chem. Phys. **100**, 7707 (1994).
[22] M. Schoen, Ber. Bunsenges. Phys. Chem. **100**, 1355 (1996).
[23] M. Schoen, C. L. Rhykerd, Jr., D. J. Diestler, and J. H. Cushman, Science **245**, 1223 (1989).
[24] C. L. Rhykerd, Jr., M. Schoen, D. J. Diestler, and J. H. Cushman, Nature (London) **330**, 461 (1987).
[25] J. N. Israelachvili, P. M. McGuiggan, and A. M. Homola, Science **240**, 189 (1988).
[26] M. Gee, P. M. McGuiggan, J. N. Israelachvili, and A. M. Homola, J. Chem. Phys. **93**, 1895 (1990).
[27] R. Yang, D. F. Evans, and W. A. Hendrickson, Langmuir **11**, 211 (1995).
[28] P. E. Sheehan and C. M. Lieber, Science **272**, 158 (1996).
[29] W. Koch, S. Dietrich, and M. Napiórkowski, Phys. Rev. E **51**, 3300 (1995).
[30] P. Röcken and P. Tarazona, J. Chem. Phys. **105**, 2043 (1996).
[31] M. P. Allen and D. J. Tildesley, *Computer Simulation of Liquids* (Clarendon, Oxford, 1987).
[32] I. N. Bronstein and K. A. Semendjajew, *Taschenbuch der Mathematik* (B. G. Teubner Verlagsgesellschaft, Stuttgart, 1991).
[33] M. Schoen, J. Comput. Phys. **118**, 159 (1995).
[34] W. H. Press, B. P. Flannery, S. A. Teukolsky, and W. T. Vetterling, *Numerical Recipes in FORTRAN* (Cambridge University, Cambridge, England, 1990), Chap. 3.
[35] D. J. Diestler, M. Schoen, J. E. Curry, and J. H. Cushman, J. Chem. Phys. **100**, 9140 (1994).
[36] D. J. Diestler and M. Schoen, Acta Chim. Hungar. Models in Chemistry **132**, 45 (1995).
[37] D. A. McQuarrie, *Statistical Mechanics* (Harper & Row, New York, 1976).
[38] J. P. Hansen and I. R. McDonald, *Theory of Simple Liquids*, 2nd ed. (Academic, London, 1986).
[39] T. L. Hill, *Statistical Mechanics* (Dover, New York, 1987), Chap. 6.
[40] M. Schoen, Physica A **240**, 328 (1997).
[41] G. Arfken, *Mathematical Methods for Physicists* (Academic, London, 1985), p. 478.
[42] J. E. Curry, J. H. Cushman, M. Schoen, and D. J. Diestler, Mol. Phys. **81**, 1059 (1994).
[43] W. Koch, Ph.D. thesis, Bergische Universität Wuppertal, 1993, Chap. 5.3.
[44] M. Schoen and D. J. Diestler, Chem. Phys. Lett. **270**, 339 (1997); in the caption of Fig. 2 of this article the symbols referring to homogeneous *s* pore and heterogeneous chemically striped pore should be interchanged.
[45] J. S. Rowlinson and B. Widom, *Molecular Theory of Capillarity* (Clarendon, Oxford, 1982), Chap. 6.3.
[46] M. Schoen, S. Hess, and D. J. Diestler, Phys. Rev. E **52**, 2587 (1995).
[47] See Fig. 4 in H. Nakanishi and M. E. Fisher, J. Chem. Phys. **78**, 3279 (1983).
[48] M. Thommes and G. H. Findenegg, Langmuir **10**, 4270 (1994).
[49] M. Schoen, M. Thommes, and G. H. Findenegg, J. Chem. Phys. **107**, 3262 (1997).